Non-negative constrained inversion approaches for unmixing chromophores in multispectral optoacoustic tomography

Lu Ding[a], Xosé Luís Deán-Ben[a], Neal C. Burton[b], Robert W. Sobol[c], Vasilis Ntziachristos[a], and Daniel Razansky[a]

[a]Technical University of Munich and Helmholtz Center Munich, IngolstädterLandstraße 1, 85764 Neuherberg, Germany
[b]iThera Medical GmbH, Munich, Germany
[c]University of Pittsburgh School of Medicine, Pittsburgh, PA, USA

ABSTRACT

Due to modeling and experimental imperfections, multispectral optoacoustic tomography images are often afflicted with negative values, which are further amplified when propagating into the spectrally unmixed images of chromophore concentrations. Since negative values have no physical meaning, accuracy can potentially be improved by imposing non-negativity constraints on the initial reconstructions and the unmixing steps. Herein, we compare several non-negative constrained approaches with reconstruction and spectral unmixing performed separately or combined in a single inverse step. The quantitative performance and sensitivity of the different approaches in detecting small amounts of spectrally-distinct chromophores are studied in tissue-mimicking phantoms and mouse experiments.

Keywords: Optoacoustic/photoacoustic tomography, multispectral imaging, spectral unmixing, non-negative constraint

1. INTRODUCTION

Multispectral optoacoustic tomography (MSOT) renders the distribution of spectrally-distinctive optical absorbers deep inside scattering tissues.[1–5] Images representing the distribution of absorbing substances are commonly obtained via a two-step procedure.[6] First, the optical absorption distribution within the tissue is separately reconstructed for each illumination wavelength. Subsequently, contributions of the different absorbers (chromophores) are separated via a multispectral unmixing algorithm.

Due to experimental and modeling imperfections, negative values often appear in both the reconstructed optical absorption images and the spectrally unmixed images. Since negative values have no physical meaning, accuracy and quantitativeness can potentially be improved by imposing non-negativity constraints on the reconstruction and unmixing steps. With these additional constraints, the reconstruction and unmixing problems can no longer be considered linear transformations, thus the final result greatly depends on the particular model and on the imposed constraints.

Herein, we compare several non-negative constrained approaches where reconstruction and unmixing are either combined in a single inverse step or solved as separate problems. The results are further compared to the equivalent unconstrained approaches. The quantitative reconstruction performance and sensitivity of the different methods in detecting small chromophore concentrations is tested in tissue-mimicking phantoms and with real mouse imaging data. Our results allow establishing the most efficient methods for resolving the spatial distribution of spectrally-distinct absorbing substances.

Further author information: (Send correspondence to D.R.)
D.R.: E-mail: dr@tum.de

Photons Plus Ultrasound: Imaging and Sensing 2017, edited by Alexander A. Oraevsky, Lihong V. Wang, Proc. of SPIE Vol. 10064, 100641B · © 2017 SPIE · CCC code: 1605-7422/17/$18 · doi: 10.1117/12.2252807

2. THEORY

In this section, we describe the theoretical basis of MSOT. We introduce the linear forward model used for the reconstruction of the optical absorption and the linear unmixing model used for multi-spectral unmixing. Based on these forward models, we formulate least-squares problems which can be solved with and without additional non-negativity constraints.

2.1 Model-based Reconstruction

Model-based reconstruction makes use of a discrete linear model that maps the energy absorbed at different pixel locations after excitation with a laser pulse to the time-sampled pressure signals observed at the ultrasonic transducers. This linear model is derived from the optoacoustic wave equation, which under the thermal and stress confinement conditions and for excitation with a Dirac impulse, is given by[7]

$$\frac{\partial^2 p(\boldsymbol{r},t)}{\partial t^2} - c^2\nabla^2 p(\boldsymbol{r},t) = \Gamma H(\boldsymbol{r})\frac{\partial \delta(t)}{\partial t}, \tag{1}$$

where Γ is the dimensionless Grüneisen parameter, c is the speed of sound in the medium and $H(\boldsymbol{r})$ is the amount of energy absorbed in the tissue per unit volume. The analytical solution of the wave equation (1) is given by the Poisson-type integral[7]

$$p(\boldsymbol{r},t) = \frac{\Gamma}{4\pi c}\frac{\partial}{\partial t}\int\limits_{S(\boldsymbol{r},ct)} \frac{H(\boldsymbol{r}')}{|\boldsymbol{r}-\boldsymbol{r}'|}d\boldsymbol{r}', \tag{2}$$

where $S(\boldsymbol{r},ct)$ denotes the sperical surface with center $\boldsymbol{r}$ and radius ct. That is, integration is performed along the spherical surface for which $|\boldsymbol{r}-\boldsymbol{r}'| = ct$. For a cross-sectional (two-dimensional) acquisition geometry, the solution simplifies to[8]

$$p(\boldsymbol{r},t) \approx \frac{\Gamma}{4\pi c}\frac{\partial}{\partial t}\int\limits_{L(\boldsymbol{r},ct)} \frac{H(\boldsymbol{r}')}{|\boldsymbol{r}-\boldsymbol{r}'|}d\boldsymbol{r}', \tag{3}$$

where $L(\boldsymbol{r},ct)$ is a circumference with radius ct.

The linear relationship between pressure and absorption in (3) needs to be discretized to apply numerical reconstruction methods. One discretization approach which allows for efficient implementation of the reconstruction has been proposed recently in.[9] The discretization procedure leads to the desired discrete linear forward model

$$\boldsymbol{p} = \boldsymbol{A}\boldsymbol{h}, \tag{4}$$

with a model matrix $\boldsymbol{A}$ that relates the optical absorption at all pixels in $\boldsymbol{h}$ to the time-discrete, stacked pressure signals at all transducers in $\boldsymbol{p}$. To reconstruct the absorption $\boldsymbol{h}$ from actually measured pressure signals $\boldsymbol{p}_m$, we solve the least-squares problem

$$\hat{\boldsymbol{h}} = \arg\min_{\boldsymbol{h}} \|\boldsymbol{A}\boldsymbol{h} - \boldsymbol{p}_m\|_2^2. \tag{5}$$

A regularization term might be added to the cost function in (5), but is usually unnecessary for a two-dimensional setup with sufficient angular coverage.[10] The solution to the least-squares problem is given by

$$\hat{\boldsymbol{h}} = \boldsymbol{A}^+\boldsymbol{p}_m, \tag{6}$$

where $\boldsymbol{A}^+$ denotes the Moore-Penrose pseudoinverse of $\boldsymbol{A}$.

2.2 Linear Unmixing

In MSOT, image acquisition is done for multiple wavelengths. For different wavelengths, we get different images of the optical absorption. The absorption coefficient $\mu_a(\lambda,\boldsymbol{r})$ at a location $\boldsymbol{r}$ for a wavelength λ is given by the molar extinction coefficients of the absorbing substances $\varepsilon_j(\lambda)$, $j = 1, \ldots, S$, weighted by their concentration $c_j(\boldsymbol{r})$ at that location

$$\mu_a(\lambda,\boldsymbol{r}) = \sum_{j=1}^{S} \varepsilon_j(\lambda)c_j(\boldsymbol{r}). \tag{7}$$

The optical absorption is then given by

$$h(\lambda, \boldsymbol{r}) = \Phi(\lambda, \boldsymbol{r})\mu_a(\lambda, \boldsymbol{r}), \tag{8}$$

where $\Phi(\lambda, \boldsymbol{r})$ is the local light fluence for wavelength λ. Since the light fluence is difficult to measure or estimate, we use the common simplification to assume that the spectral variations in $\Phi(\lambda, \boldsymbol{r})$ are negligible compared to those in the $\varepsilon_j(\lambda)$. That is $\Phi(\lambda, \boldsymbol{r}) = \Phi(\boldsymbol{r})$.

Let $\boldsymbol{\Phi}$ denote the vector containing the light fluence at all pixel locations, $\boldsymbol{H} = [\boldsymbol{h}(\lambda_1), \ldots, \boldsymbol{h}(\lambda_W)]$ the matrix that contains the optical absorption images for different measured wavelengths λ_i and $\boldsymbol{c}_j$ the vector that contains the concentrations of substance j at all pixel locations. With the matrix of all extinction coefficients

$$\boldsymbol{E} = \begin{bmatrix} \varepsilon_1(\lambda_1) & \cdots & \varepsilon_1(\lambda_W) \\ \vdots & \ddots & \vdots \\ \varepsilon_S(\lambda_1) & \cdots & \varepsilon_S(\lambda_W) \end{bmatrix} \tag{9}$$

and the matrix that contains the Hadamard products of fluence and concentration $C = [\boldsymbol{c}_1 \odot \boldsymbol{\Phi}, \ldots, \boldsymbol{c}_S \odot \boldsymbol{\Phi}]$, we can finally write the optical absorption as

$$\boldsymbol{H} = \boldsymbol{C}\boldsymbol{E}. \tag{10}$$

To perform unmixing of the (weighted) concentration images of the different substances given the previously reconstructed images of the optical absorption, we solve another least squares problem

$$\hat{\boldsymbol{C}} = \arg\min_{\boldsymbol{C}} \|\boldsymbol{C}\boldsymbol{E} - \hat{\boldsymbol{H}}\|_2^2 \tag{11}$$

with the solution

$$\hat{\boldsymbol{C}} = \hat{\boldsymbol{H}}\boldsymbol{E}^+ = \boldsymbol{A}^+\boldsymbol{P}_m\boldsymbol{E}^+, \tag{12}$$

where $\boldsymbol{P}_m = [\boldsymbol{p}_m(\lambda_1), \ldots, \boldsymbol{p}_m(\lambda_W)]$ collects the pressure signals measured at different wavelengths.

Note that, since matrix multiplication is associative, the order of unmixing and reconstruction can be exchanged. In fact, the reconstructed absorption in (12) is the solution to the combined (reconstruction and unmixing) least-squares problem

$$\hat{\boldsymbol{C}} = \arg\min_{\boldsymbol{C}} \|\boldsymbol{A}\boldsymbol{C}\boldsymbol{E} - \boldsymbol{P}_m\|_2^2. \tag{13}$$

Thus, directly solving the combined problem based on linear model that maps the concentrations to the pressure signals

$$\boldsymbol{P} = \boldsymbol{A}\boldsymbol{C}\boldsymbol{E} \tag{14}$$

or solving reconstruction and unmixing separately yields equivalent results. However, if additional constraints are taken into account, such as a non-negativity constraint, the results are no longer the same.

2.3 Non-negative Constrained Approaches

Since negative values have no physical meaning, we can apply non-negative constraints to any of the previously introduced inversion problems to improve the reconstruction quality. For example, for the tomographic reconstruction problem, we simply add a non-negativity constraint to the least-squares problem to get

$$\hat{\boldsymbol{H}} = \arg\min_{\boldsymbol{H} \geqslant \boldsymbol{0}} \|\boldsymbol{A}\boldsymbol{H} - \boldsymbol{P}_m\|_2^2. \tag{15}$$

The subsequent non-negative constrained unmixing problem is given by

$$\hat{\boldsymbol{C}} = \arg\min_{\boldsymbol{C} \geqslant \boldsymbol{0}} \|\boldsymbol{C}\boldsymbol{E} - \hat{\boldsymbol{H}}\|_2^2. \tag{16}$$

On the other hand, we can also formulate the combined problem as a non-negative constrained inversion problem

$$\hat{\boldsymbol{C}} = \arg\min_{\boldsymbol{C} \geqslant \boldsymbol{0}} \|\boldsymbol{A}\boldsymbol{C}\boldsymbol{E} - \boldsymbol{P}_m\|_2^2. \tag{17}$$

Note that $\boldsymbol{C} \geqslant \boldsymbol{0}$ implies that $\boldsymbol{H} = \boldsymbol{CE} \geqslant \boldsymbol{0}$ since all entries in $\boldsymbol{E}$ are non-negative. The results of (16) and (17) will be different due to the non-linearities resulting from the non-negativity constraints. The total residual, i.e., $\|\boldsymbol{ACE} - \boldsymbol{P}_m\|_2^2$ will be lower with the solution to (17) since this solution actually minimizes the residual for all non-negative concentrations. Separate processing, however, has advantages in terms of computational complexity and is easily parallelized. As hybrid approach, non-negative constraints can be imposed solely on certain columns of $\boldsymbol{C}$ corresponding to the optical absorbers of interest.

Note that, the non-negative constraint is not applicable for the purpose of signal unmixing prior to reconstructions since $\boldsymbol{P}$ and $\boldsymbol{PE}^+$ might indeed have negative entries.

3. METHODS

In the previous section we have seen that non-negativity constraints can be added to different reconstruction and unmixing problems. If those constraints are introduced and unmixing and reconstruction are done consecutively, also the order matters. The relevant combinations are

- Constrained reconstruction followed by constrained unmixing (CR-CM)
- Constrained reconstruction followed by unconstrained unmixing (CR-UM)
- Unconstrained reconstruction followed by constrained unmixing (UR-CM)
- Unconstrained reconstruction followed by unconstrained unmixing (UR-UM), which is identical to solving combined unconstrained problem
- Unmixing of the pressure signals followed by constrained reconstruction (UM-CR)
- Combined and constrained reconstruction and unmixing (CB1)
- Combined reconstruction and unmixing with a non-negative constraint only imposed on the contrast agent of interest (CB2)

The unconstrained reconstruction problems are solved with the iterative LSQR method[11] while the unconstrained unmixing problems are solved directly, which is possible due to the small size of $\boldsymbol{E}$. The constrained problems with large dimensionality, i.e., the combined problems and the constrained reconstruction, are solved using an efficient method for large non-negative constrained least-squares problems[12] and the low-dimensional constrained unmixing problems are solved with the fnnls method.[13]

The reconstruction performance of the given methods was analyzed experimentally in different setups with different chromophores and contrast agents. The experiments were done with a commercial small animal multispectral optoacoustic tomography scanner (Model: MSOT256-TF, iThera Medical GmbH, Munich, Germany) which contains a wavelength-tunable (680-950nm) laser.

3.1 Phantom Experiment

In our first experimental, we imaged a cylindrical agar phantom with an diameter of 19mm, which contained India Ink and Intralipid to mimick tissue background. We inserted two tubings at different depths, with varying concentrations of AlexaFluor 750 (InvitrogenTM) measured by a spectrophotometer. We captured pressure signals at 11 different wavelengths from 700 to 800 nm.

3.2 *In Vivo* Mouse Experiments

To assess the reconstruction performance in more realistic conditions, we use a similar setup but replace the phantom with a mouse. All procedures involving animal care and experimentation were conducted according to the guidelines of the Helmholtz Center Munich and the government of Upper Bavaria and complied with German federal and international laws and regulations. The *in vivo* mouse experiment was terminal.

In the *in vivo* experiment, we inserted a polyethylene tubing into the rectum of the mouse. Then analogously to the phantom experiment, we injected AlexaFluor 750 with different concentrations into the tubing. For each concentration, cross-sectional images were taken at 10 different positions. Pressure signals were recorded at 22 wavelengts from 690 to 900 nm.

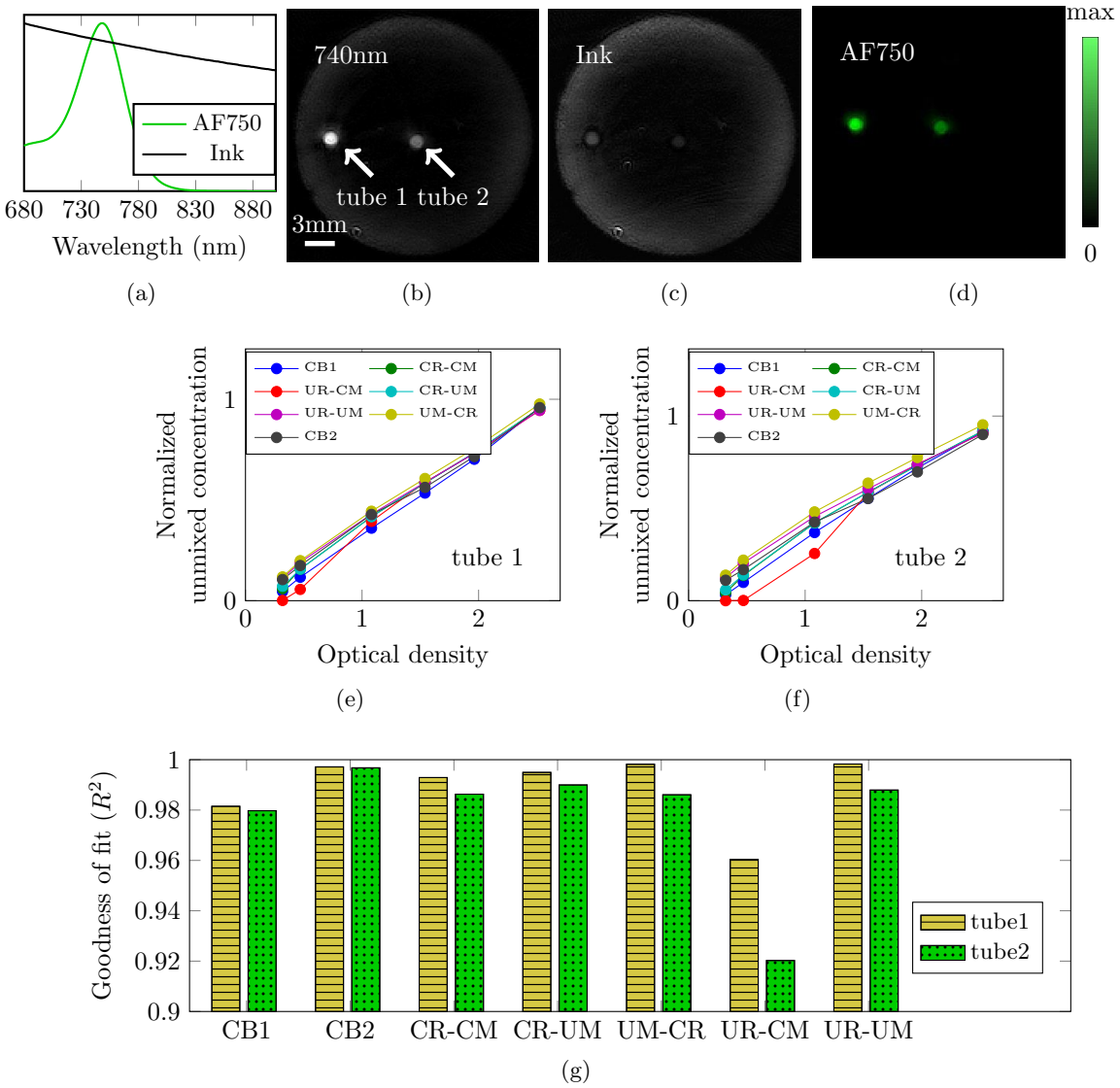

Figure 1. Unmixing results for the phantom with background ink absorption and two insertions (tubes) containing the AF750 dye. a)Spectra of AF750 and ink. b) Optoacoustic image acquired at 740 nm with 2.5 OD of AF750 insertion. c) Unmixed image corresponding to the ink component obtained with the CR-CM method. d) Unmixed image corresponding to the AF750 component obtained with the CR-CM method. e)-f) Pixel values of the unmixed image within the tubes as a function of the optical density of AF750. g) The R^2 values, representing quality of the linear fit in e) and f).

4. RESULTS

Results from the phantom experiment are summarized in Fig. 1. Fig. 1a) shows the normalized extinction coefficients of the background (Ink) and the contrast agend (AF750). The reconstructed optical absorption at a wavelength of 740 nm is depicted in Fig. 1b) and the unmixed concentrations are depicted in Fig. 1c) and d). Here we show the result of unmixing for the CR-CM method, i.e., separate constrained reconstruction followed by constrained unmixing.

The distribution of AF750 is confined within the tubings and no cross-talk artifacts are visible. The deeper tubing exhibits a lower amplitude due to the light fluence attenuation. In the unmixed image of the Ink concentration, we get a non-zero concentration at the position of the tubings, i.e., cross-talk artifacts are visible. To evaluate the accuracy of the unmixing without knowledge of the light-fluence, we inject different concentrations

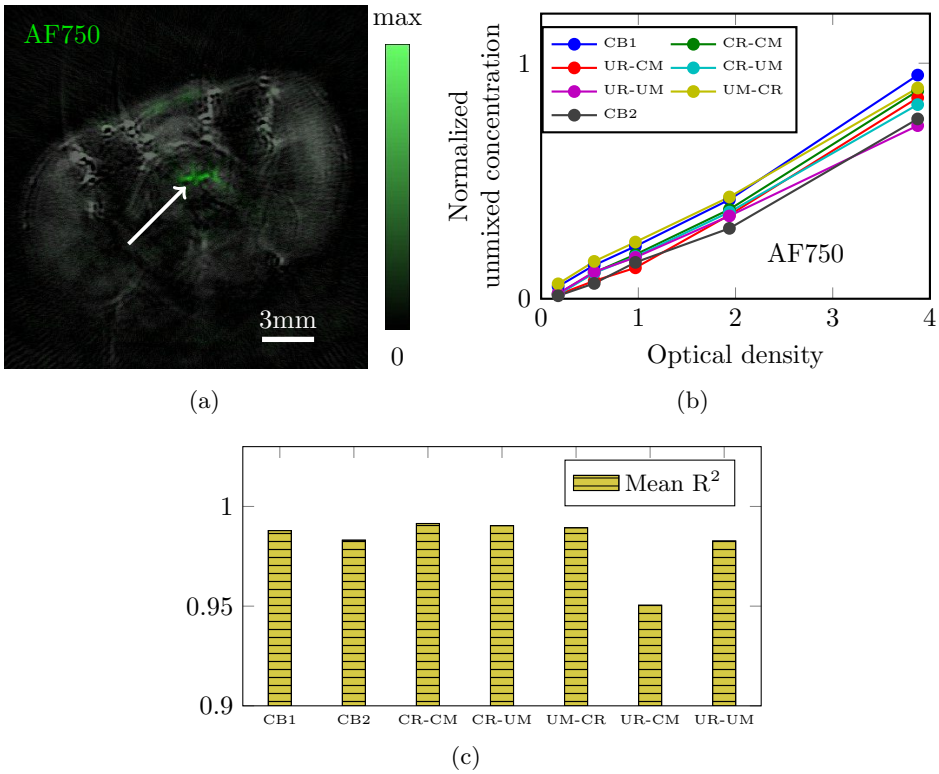

Figure 2. Unmixing results for the *in vivo* mouse experiment. a) Unmixed distribution of AF750 obtained with the CR-CM method. b) Unmixed optoacoustic signal within the tubes as a function of the optical density of AF750. c) Mean R^2 value of the linear fit of the curves in b) averaged over all 10 imaged cross-sections.

of the contrast agent into the tubing and then evaluate how close the resulting unmixed concentration comes to the desired linear behavior. In Figures 1e) and f) we show the average unmixed concentration inside the two tubings with respect to the actual concentration for the different unmixing/reconstruction methods. We observe that all methods show similar linear behavior, with exception of the UR-CM method which shows strongly non-linear behavior for low concentrations. This assessment is confirmed by the goodness of a linear fit to the concentration curves which is depicted in Fig. 1g). We note that the result for the deeper tubing is always worse due to the lower signal strength. The CB2 method exhibits the best linearity, however, the difference to most other methods is minor.

The results of the *in vivo* mouse experiment are shown in Fig. 2. In short, the conclusions are similar as for the phantom experiment. A representative unmixed image of AF750 is shown in Fig. 2a) superimposed onto the image of the optical absorption taken at 800 nm. Same as for the phantom experiment, we show the concentrations within the tubing obtained from the different methods with respect to the actual concentrations in Fig. 2b). The unmixed concentrations are averaged over the ten different cross-sections of the mouse. The goodness of the linear fits is presented in Fig. 2c). Again the UR-CM method clearly shows the worst performance.

5. DISCUSSION AND CONCLUSIONS

In model-based reconstruction for optoacoustic tomography, errors in the forward model due to approximations and simplifications as well as noise lead to artifacts in the resulting images, such as physically meaningless negative values. For multispectral optoacoustic tomography, the negative values appear in both the optoacoustic reconstruction and the spectral unmixing steps. In this work, we analyzed multiple methods which impose non-negativity constraints on the reconstructed optical absorption as well as the unmixed concentrations.

For an accurate model where the acquisition noise is the main detrimental factor for image quality, the method that yields the lowest residual should also yield the most accurate images. However, while the method that solves

the constrained combined problem in (17) (CB1) yields the lowest residual for any non-negative concentration, it does not consistently outperform the other approaches. In our experiments, all methods except the UR-CM method perform similarly. The combined approach (CB1) might be preferable once various remaining issues with the forward model, such as the light fluence calculation have been solved in future work. Another interesting aspect for future work would be to analyse other performance measures and see if we come to the same conclusion.

ACKNOWLEDGMENTS

D.R. acknowledges grant support from the European Research Council under Consolidator Grant ERC-2015-CoG-682379 and Human Frontier Science Program (HFSP) Grant RGY0070/2016.

REFERENCES

[1] Razansky, D., Distel, M., Vinegoni, C., Ma, R., Perrimon, N., Köster, R. W., and Ntziachristos, V., "Multispectral opto-acoustic tomography of deep-seated fluorescent proteins in vivo," *Nature Photonics* **3**(7), 412–417 (2009).

[2] Yao, J. and Wang, L. V., "Photoacoustic tomography: fundamentals, advances and prospects," *Contrast media & molecular imaging* **6**(5), 332–345 (2011).

[3] Jeon, M., Kim, J., and Kim, C., "Multiplane spectroscopic whole-body photoacoustic imaging of small animals in vivo," *Medical & biological engineering & computing* **54**(2-3), 283–294 (2016).

[4] Nie, L. and Chen, X., "Structural and functional photoacoustic molecular tomography aided by emerging contrast agents," *Chemical Society Reviews* **43**(20), 7132–7170 (2014).

[5] Deán-Ben, X. L. and Razansky, D., "Adding fifth dimension to optoacoustic imaging: volumetric time-resolved spectrally enriched tomography," *Light: Science & Applications* **3**(1), e137 (2014).

[6] Luke, G. P., Nam, S. Y., and Emelianov, S. Y., "Optical wavelength selection for improved spectroscopic photoacoustic imaging," *Photoacoustics* **1**(2), 36–42 (2013).

[7] Cox, B., Kara, S., Arridge, S., and Beard, P., "k-space propagation models for acoustically heterogeneous media: Application to biomedical photoacoustics," *The Journal of the Acoustical Society of America* **121**(6), 3453–3464 (2007).

[8] Rosenthal, A., Razansky, D., and Ntziachristos, V., "Fast semi-analytical model-based acoustic inversion for quantitative optoacoustic tomography," *IEEE transactions on medical imaging* **29**(6), 1275–1285 (2010).

[9] Ding, L., Dean-Ben, X. L., and Razansky, D., "Real-time model-based inversion in cross-sectional optoacoustic tomography," *Medical Imaging, IEEE Transactions on* **35**(8), 1883–1891 (2016).

[10] Buehler, A., Rosenthal, A., Jetzfellner, T., Dima, A., Razansky, D., and Ntziachristos, V., "Model-based optoacoustic inversions with incomplete projection data," *Medical physics* **38**(3), 1694–1704 (2011).

[11] Paige, C. C. and Saunders, M. A., "Lsqr: An algorithm for sparse linear equations and sparse least squares," *ACM transactions on mathematical software* **8**(1), 43–71 (1982).

[12] Ding, L., Deán-Ben, X. L., Lutzweiler, C., Razansky, D., and Ntziachristos, V., "Efficient non-negative constrained model-based inversion in optoacoustic tomography," *Physics in medicine and biology* **60**(17), 6733 (2015).

[13] Bro, R. and De Jong, S., "A fast non-negativity-constrained least squares algorithm," *Journal of chemometrics* **11**(5), 393–401 (1997).